An R-matrix study of singlet and triplet continuum states of N_2

2014 J. Phys. B: At. Mol. Opt. Phys. 47 105204

(http://iopscience.iop.org/0953-4075/47/10/105204)

IOP Publishing Journal of Physics B: Atomic, Molecular and Optical Physics

J. Phys. B: At. Mol. Opt. Phys. **47** (2014) 105204 (13pp) doi:10.1088/0953-4075/47/10/105204

An R-matrix study of singlet and triplet continuum states of N_2

Duncan A Little and Jonathan Tennyson

Department of Physics and Astronomy, University College London, Gower Street London, WC1E 6BT, UK

E-mail: duncan.little.11@ucl.ac.uk

Received 10 January 2014, revised 7 April 2014
Accepted for publication 11 April 2014
Published 7 May 2014

Abstract

A systematic calculation of the positions and widths of the resonances converging on the first two excited states of N_2^+ ($A\ ^2\Pi_u$ and $B\ ^2\Sigma_u^+$) is presented. A closely-spaced grid of geometries is used to give continuous resonance curves without the need for curve fitting. Three methods, fitting the eigenphase sum, the time-delay method and the R-matrix specific QB method, are tested. Fits to the longest three time-delays are found to give the most reliable and complete determination of the resonance parameters. The low excitation energies of the A and B ion states results in complex resonance features with many avoided crossings leading to pronounced structures in both the resonance curves and the associated widths. The resonance curves likely to be important for dissociative recombination are identified. Their positions generally agree well with the calculations of Guberman, although in some cases their widths are narrower. Full data on all curves is provided.

Keywords: resonances, dissociative recombination, time-delay

S Online supplementary data available from stacks.iop.org/JPhysB/47/105204/mmedia

(Some figures may appear in colour only in the online journal)

1. Introduction

Molecular nitrogen, N_2, is a strongly bound diatomic molecule that makes up not only the majority of the terrestrial atmosphere but also that of Titan and Triton. The characterization of N_2 and N_2^+ is essential for correctly describing processes that occur within these atmospheres and associated ionospheres. This considered, there is a surprising lack of data, experimental or theoretical, on electronic states of N_2 other than that of $^1\Sigma_u^+$ and $^1\Pi_u$ symmetry. We (Little and Tennyson 2013) recently computed a comprehensive set of *ab initio* singlet and triplet potential energy curves (PECs) describing the Rydberg states that converge upon the ground state of N_2^+ for $\ell \leqslant 4$ and $n \leqslant 6$. In this work we extend our calculation to the quasi-bound or resonance states lying in the continuum above the ion ground state and characterize the position and width (lifetime) of resonant states with both valence and Rydberg character.

Resonances lead to large variations in the cross-sections of electron scattering processes and need to be treated carefully if these processes are to be described correctly. Resonances can also provide a route to dissociation of molecular ions through dissociative recombination (DR) (Larsson and Orel 2008). The DR of N_2^+ can be described as,

$$N_2^+ + e^- \rightarrow N_2^{**} \rightarrow N + N. \quad (1)$$

In this study we focus on the resonant states of the electron—N_2^+ collision system, denoted N_2^{**} in equation (1), which could facilitate this process. Experimentally there have been a number of studies (Mehr and Biondi 1969, Mahdavi *et al* 1971, Cunningham and Hobson 1972, Mul and McGowan 1979, Canosa *et al* 1991, Geoghegan *et al* 1991, Zipf 1980, Peterson *et al* 1998, Sheehan and St-Maurice 2004) however, difficulties cooling the N_2^+ ion to the vibrational ground state means that the results are inconsistent when compared to a molecule of similar size, for example, O_2^+ (Larsson and Orel 2008).

Previous *ab initio* studies characterizing states above the ion ground state can be separated into two categories: PEC calculations using quantum chemical methods, for which

care is required (Stibbe and Tennyson 1999), and scattering calculations. Guberman 2003, 2007, 2012, 2013 calculated PECs for their specific use in DR calculations using a multi-reference configuration interaction (MRCI) approach with the quantum chemistry package MOLPRO (Werner *et al* 2010). Our previous study (Little and Tennyson 2013) showed that while the representation of valence states given by an MRCI calculation is good, this approach does not give the same comprehensive information on the Rydberg states when compared to a scattering calculation. Additionally, it is difficult to produce a self-consistent model using an MRCI calculation. Orbitals must be tailored for each symmetry to produce correct results. The ion ground state is not explicitly included in the calculation in the way that is inherent to a scattering calculation. For DR the relative placement of the ion curve and neutral states can have a significant effect on the cross-section. In particular, the magnitude of the cross-section is extremely sensitive to the point at which a neutral dissociative state crosses the ion ground state.

Electron-molecule scattering calculations use the ionic target as the starting point of the calculation allowing all parameters to be determined self-consistently from this reference point. Orel *et al* (1990) calculated electronic impact cross-sections for the $X\ ^2\Sigma_g^+ \rightarrow B\ ^2\Sigma_u^+$ transition at a single geometry using the complex-Kohn variational method. An R-matrix calculation by Ballance *et al* (1998) found Rydberg-type resonances of $^{1,3}\Sigma_g^+$ symmetry, this work was extended by Nagy (Nagy *et al* 1999, Nagy 2003) to include vibrational motion to determine vibronic electron impact excitation cross-sections for the $X \rightarrow B$ transition. These calculations are in the spirit of a conventional scattering calculation; a single or small number of appropriate geometries are calculated to determine a scattering parameter which, in general, only depends on these internuclear separations. In this study we calculate resonant states at a large number of separations to make up sets of PECs for each symmetry with singlet and triplet spin.

This paper presents a comprehensive set of curves for singlet and triplet valence and Rydberg states of N_2 up to g-wave character above the ionization threshold. All calculations were performed using R-matrix based scattering calculations, three different methods of resonance detection and fitting were explored. The final calculations used the time-delay method of Smith (1960) as implemented by Stibbe and Tennyson (1996) with improvements to the fitting method.

2. Method

Resonant state calculations were performed using the recently-updated UKRmol code suite (Carr *et al* 2012). These combine *ab initio* quantum chemistry methods with scattering theory to model electron-molecule collisions. The molecular R-matrix and UKRmol codes have been extensively reviewed elsewhere (Tennyson 2010), so only key points will be discussed here.

The R-matrix method partitions space into an 'inner' region with $r \leqslant a$ and an 'outer' region with $r > a$. The two are linked by using energy-independent information from the inner region to construct the energy-dependent R-matrix on a sphere of radius a. In the inner region the scattering electron is indistinguishable from the electrons of the target molecule meaning that correlation and exchange effects must be treated in full. In the outer region, where the scattering electron is considered as distinct, the problem is much simpler but must be solved for each scattering energy.

The inner region calculation is performed in two separate steps: first an N-electron target calculation which only considers the target molecule electrons, and then an $(N+1)$-electron target plus scattering electron calculation which gives a full description of the target interacting with the scattering electron. The results of these two calculations form the input for the outer region where scattering observables, starting from K-matrices, are computed.

In the inner region, the energies are discretized and the wavefunction is given by:

$$\Psi_k^{N+1}(x_1,\ldots,x_{N+1}) = \mathcal{A}\sum_{ij} a_{ijk}\phi_i^N(x_1,\ldots,x_N)u_{ij}(x_{N+1}) + \sum_i b_{ik}\chi_i^{N+1}(x_1,\ldots,x_{N+1}), \quad (2)$$

where ϕ_i^N is the N-electron target wave functions of the ith, state and u_{ij} is an orbital used to represent the jth continuum electron with a partial wave expansion up to some maximum value of ℓ, $\ell_{\max}$; the subscript k denotes the kth inner region wave function; $\mathcal{A}$ is an antisymmetrization operator introduced so that the inner-region electrons satisfy the Pauli principle; a_{ijk} and b_{ik} are the coefficients of expansions. χ_i are multi-centred, square, integrable functions constructed using only target orbitals; they are therefore zero on the R-matrix boundary and are usually described as L^2 configurations. The L^2 configurations allow for the relaxation of the orthogonalization between the target and continuum states of the same symmetry and here are made up of the target occupied and virtual orbitals.

3. Calculation details

Full descriptions of the model and testing of this model can be found in Little and Tennyson (2013), therefore only a brief summary of the model is given here.

3.1. Target calculation

When calculating the resonant scattering states of a molecule having a good description of the target is essential. Multi-configuration self-consistent field (MCSCF) molecular orbitals (MOs) averaged over the first four states of N_2^+ were generated with MOLPRO using the Gaussian type orbital (GTO) cc-pVQZ basis set of Dunning (1989) with a complete active space (CAS) of nine electrons distributed between two σ_g, two σ_u, one π_g, and one π_u orbtials. This CAS can be denoted $(1\sigma_g, 1\sigma_u)^4(2\sigma_g, 3\sigma_g, 2\sigma_u, 3\sigma_u, 1\pi_u, 1\pi_g)^9$. Both MOLPRO and the 'polyatomic' implementation of the UK molecular R-matrix codes (Morgan *et al* 1997) use only Abelian symmetries. All calculations were therefore performed in D_{2h} symmetry; in most cases it was straightforward to transform the results into the higher $D_{\infty h}$ symmetries. $D_{\infty h}$ symmetries are used to describe results below where assignments could be made unambiguously.

The MOs generated by MOLPRO were renormalized and reordered for use with the UKRmol code suite. The target wavefunctions were then calculated using the scattering configuration interaction (CI) program SCATCI (Tennyson 1996a), for consistency the same basis set and CAS as the MOLPRO MCSCF calculation were used. 128 target states were generated initially, this was then reduced to the lowest 100 for $(N+1)$-electron inner region calculation. The agreement with experimental values for the ground and first two excited states ($X\,^2\Sigma_g^+$, $A\,^2\Pi_u$ and $B\,^2\Sigma_u^+$) is excellent; see Little and Tennyson (2013) for a comparison with other data.

3.2. $(N+1)$-electron inner region calculation

The $(N+1)$-electron inner region calculation is, in essence, the target molecule calculation extended to accommodate a scattering electron. The scattering electron is represented by continuum orbitals which take the form of bond-centred GTOs fitted to Bessel functions with $\ell \leqslant 4$ (Faure *et al* 2002). The MOs generated for the target were also used for the $(N+1)$-electron calculation. The continuum orbitals are Schmidt orthoganalized to the target MOs and then just the continuum orbitals are symmetric-orthoganalized so that all orbitals are orthogonal. The CAS for the $(N+1)$-electron calculation was augmented with 14 virtual orbitals to ($5\sigma_g$, $5\sigma_u$, $3\pi_u$, $2\pi_g$, $1\delta_u$, $1\delta_g$), where the term 'virtual orbitals' refers to target orbitals not occupied in the N or $N+1$ CAS. Extra 'uncontracted' orbitals of this form were added to equation (2); for a discussion on the details of contracted and uncontracted orbitals see Tennyson (1996b) and Dora *et al* (2009). The L^2 functions take two forms: those in which the scattering electron enters the target active space, relaxing the orthogonality between the target and contiuum orbitals and those in which the scattering electron occupies the virtual orbitals.

Although, ideally, it would not have been necessary to make modifications to the model presented in Little and Tennyson (2013) there were significant linear dependence errors in the final positions and widths of the resonant states of Σ_u^+ and Δ_u symmetry as well as the resonance states of Π_g and Φ_g symmetry. These errors occur due to the numerical nature of the orthogonilization procedure; orbitals which are effectively linear dependent have a small but non-zero eigenvalue in the overlap matrix. A deletion threshold is set at which any value below is considered to be zero (Morgan *et al* 1997). It was found that increasing the deletion threshold to 10^{-5} from the default value of 10^{-7} used in Little and Tennyson (2013) eliminated the linear dependence errors. Increasing the deletion threshold reduces the number of MOs used in the calculation, effectively reducing the size of the basis set.

As this is a variational calculation the result of this is that the energy positions of the bound states increase slightly relative to the bound states presented in Little and Tennyson (2013). There is a largely uniform shift of $\lesssim$0.01 eV; however, Rydberg states with the lowest ℓ for a given n are shifted by up to 0.1 eV. This includes Rydberg series converging on the first excited state of the ion. The stability and smoothness of these curves has also improved, indicating that the previous calculation had linear dependence errors which did not become completely apparent until we extended our calculation to the continuum. Bound states for the affected symmetries were recomputed and are included in the supplementary data (available at stacks.iop.org/JPhysB/47/105204/mmedia). The results for states we presented in tabular form in Little and Tennyson (2013) have been updated and are given in tables 1 and 2 for states converging on the X and A states respectively. For states where experimental data exists there is an overall improvement in agreement with experimental results. We recommend using this new data over that given in Little and Tennyson (2013).

Calculations were actually performed using the D_{2h} point group and singlet and triplet states for all eight D_{2h} symmetries were considered. Calculations were performed with steps of 0.001 Å to give smooth curves which did not require fitting.

3.3. Outer region resonant state calculations

After solving for the $(N+1)$-electron inner region wavefunction and target wavefunctions, the $N+1$ eigenpairs and raw boundary amplitudes are combined in an interface program to generate the information to build an R-matrix on the boundary of the R-matrix sphere. At this point all but the lowest four targets states (five in D_{2h}) are removed from the calculation. The R-matrix is then generated and propagated to a distance far enough for the results to stabilize; here a value of 300.1 a_0 was used. At this point K-matrices are generated by matching to asymptotic solutions; these are in turn used to determine the resonance states.

4. Resonance detection and fitting

In formal scattering theory a resonance is a pole in the complex S-matrix which has a non-zero real and imaginary part. The real and imaginary parts of the pole form the energy and autoionization half-width of the resonance with the following form

$$E = E^{\mathrm{r}} - i\Gamma/2 \tag{3}$$

where E is a complex energy, E^{r} is the resonance position and Γ is the autoionization width. There are a number of ways of finding the resonance position and widths (Sochi and Storey 2013). Here we consider three different methods: fitting the eigenphase sum (Hazi 1979), the QB method of Quigley and Berrington (Quigley and Berrington 1996, Quigley *et al* 1998) and the time-delay method (Stibbe and Tennyson 1996). Each will be discussed in turn below.

4.1. Fitting the eigenphase sum

Fitting of the eigenphase sum has long been the *de facto* option for resonance detection and fitting, not just for R-matrix calculations but also the complex Kohn variational method (Rescigno *et al* 1995). The eigenphase sum at a given energy is calculated from the sum of the eigenvalues of the K-matrix and resonances appear as a rapid increase of π radians as a function of increasing energy. Once a resonance has been located it can be fitted to the Breit–Wigner form (Hazi 1979),

$$\delta(E) = \delta_0(E) + \arctan\frac{\Gamma}{2(E^r - E)}, \tag{4}$$

Table 1. Equilibrium energies, E_e (eV), internuclear separations, R_e (Å), and, quantum defects, α, of Rydberg states affected by changes to the model presented in Little and Tennyson (2013) converging upon the X $^2\Sigma_g^+$ state. Comparison is made with experimental data where available. The calculated equilibrium energies are given relative to the zero point energy of the X $^2\Sigma_g^+$ state. All experimental data is from Huber and Jungen (1990) unless otherwise specified. Only T_0 is available for data from Huber and Jungen (1990) so experimental energies are given relative to the value of T_0 of the X $^2\Sigma_g^+$ state given by Lofthus and Krupenie (1977).

		This work			Experiment	Comparison[a]
Rydberg series	n	R_e	E_e	α	E_e	ΔE_e
c′$_n$ $^1\Sigma_u^+(np\sigma_u)$[b]	3	1.127	−2.5848	0.7059	−2.6346	−0.0498
	4	1.138[c]	−1.1504[c]	0.5767[c]	−1.2173	−0.0669
	5	1.127	−0.6996	0.5910	−0.7100	−0.0104
	6	1.125	−0.4654	0.5931	−0.4713	−0.0059
	7	1.124	−0.3315	0.5934	−0.3351	−0.0036
	8	1.125	−0.2481	0.5947	−0.2490	−0.0009
	9	1.125	−0.1927	0.5960	−0.1933	−0.0006
	10	1.125	−0.1539	0.5979	−0.1542	−0.0003
	11	1.125	−0.1258	0.6002	−0.1260	−0.0002
$^3\Sigma_u^+(np\sigma_u)$	3	1.125	−2.6799	0.7468	−2.6036[d]	0.0763
	4	1.124	−1.2561	0.7089		
	5	1.123	−0.7390	0.7096		
	6	1.123	−0.4892	0.7267		
	7	1.122	−0.3498	0.7667		
	8	1.121	−0.2655	0.8518		
$^1\Delta_u(nf\delta_u)$	4	1.125	−0.8512	0.0021		
	5	1.125	−0.5453	0.0050		
	6	1.125	−0.3789	0.0074		
	7	1.125	−0.2784	0.0094		
	8	1.125	−0.2132	0.0114		
	9	1.125	−0.1685	0.0137		
	10	1.125	−0.1365	0.0166		
$^3\Delta_u(nf\delta_u)$	4	1.125	−0.8514	0.0023		
	5	1.125	−0.5454	0.0055		
	6	1.125	−0.3790	0.0080		
	7	1.125	−0.2785	0.0103		
	8	1.125	−0.2133	0.0126		
	9	1.125	−0.1686	0.0154		
	10	1.125	−0.1366	0.0194		

[a] Obs. − Calc.
[b] Expt. $\alpha = 0.608\,22$, (Huber and Jungen 1990).
[c] Perturbed equilibrium position.
[d] Huber and Herzberg (1979).

Table 2. Equilibrium energies, E_e (eV), internuclear separations, R_e (Å), and, quantum defects, α, of Rydberg states affected by changes to the model presented in Little and Tennyson (2013) converging upon the A $^2\Pi_u$ state. Comparison is made with experimental data where available. The calculated equilibrium energies are given relative to the zero point energy of the X $^2\Sigma_g^+$ state. All experimental data is from Huber and Herzberg (1979).

	This work			Experiment	Comparison[a]
Rydberg state	R_e	E_e	α	E_e	ΔE_e
$^1\Pi_g(3p\sigma_u)$	1.179	−1.2191	0.6360	−1.4184	−0.1993
$^3\Delta_u(3d\pi_g)$	1.182	−0.2449	−0.0527		
$^1\Delta_u(3d\pi_g)$	1.182	−0.2333	−0.0648		
$^3\Sigma_u^-(3d\pi_g)$	1.182	−0.2213	−0.0776		
$^1\Sigma_u^-(3d\pi_g)$	1.182	−0.2191	−0.0800		

[a] Obs. − Calc.

where $\delta(E)$ is the eigenphase sum and $\delta_0(E)$ the background eigenphase. This form is explicitly appropriate for a single, isolated resonance. Breit–Wigner eigenphase fitting is implemented in the program RESON (Tennyson and Noble 1984) which is integrated within the UKRmol code suite. RESON scans $\delta(E)$ for points in which there is a change in sign of the numerically computed second derivative $\frac{d^2E}{d\delta^2}$. A new finer grid is constructed around the point of inflection and fitted with the Breit–Wigner form. This approach has the advantage of being automatic and computationally inexpensive: the resonances can be found rapidly with a fairly sparse energy grid and then the points of most importance computed.

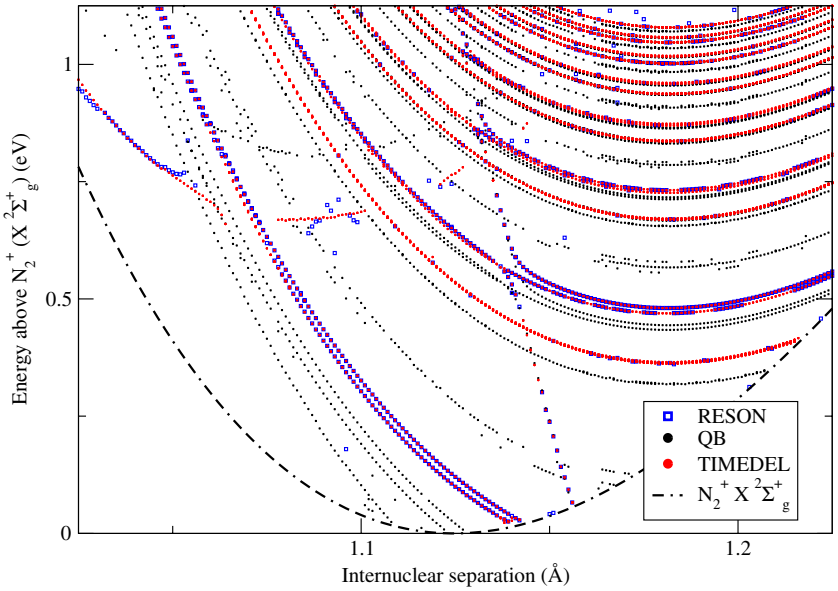

Figure 1. Comparison of the three different detection and fitting methods tested by resonance position. TIMEDEL gives the most comprehensive description of the resonant states followed by QB. RESON is subject to many false and missed detections. TIMEDEL and RESON give the same resonance positions as they are calculated using the same set of K-matrices. QB uses analytical K-matrices which are found using approximations which are not accurate for N_2; this is evident by the systematic shift in resonance position when compared to TIMEDEL and RESON.

For neutral systems this approach is fast and reliable as there are few resonances which are generally well spaced in energy. For positively charged targets however, where there are many resonances often very close in energy, for example Rydberg states, this method runs into difficulty. Resolving multiple resonances close in energy and with varying width is problematic, often resonances are poorly fitted or missed see figures 1 and 2.

4.2. Time-delay method

The time-delay method was originally proposed by Smith (1960) as an alternative method of characterizing resonances. The method has come under scrutiny recently (Shimamura *et al* 2006, Shimamura 2011, 2012) and has been applied successfully to a number a systems with many overlapping resonances (Rabadán *et al* 1998, Baccarelli *et al* 2009, Masin and Gorfinkiel 2012). Shimamura, in particular, formally extended the fitting method to include multiple overlapping resonances. In his approach resonances are parametrized by a mixing parameter β which describes the level of avoidance between two eigenvalues of the time-delay matrix, $\mathbf{Q}$, defined below. An expression is then derived to fit these two resonances as they overlap with each other. We have applied a similar extension to our fitting method.

In classical terms the time-delay can be thought of as the difference in time an electron experiences with or without an interaction with the target. The time-delay matrix is formed from the scattering matrix, $\mathbf{S}$, and the time operator, $-i\hbar\frac{\mathrm{d}}{\mathrm{d}E}$:

$$\mathbf{Q} = -i\hbar\mathbf{S}^*\frac{\mathrm{d}\mathbf{S}}{\mathrm{d}E}. \tag{5}$$

The largest eigenvalue of $\mathbf{Q}$, q_1, represents the longest time-delay of the incident electron. If q_1 is plotted against energy, resonances appear as Lorentzians which can be fitted for position and width. The time-delay method was implemented in the R-matrix method by Stibbe and Tennyson (1996) using the module TIMEDEL (Stibbe and Tennyson 1998). TIMEDEL fits the first eigenvalue of the $\mathbf{Q}$ matrix as a function of energy using a Lorentzian of the form:

$$q_1(E) = \frac{\Gamma}{(E - E^{\mathrm{r}})^2 + (\Gamma/2)^2}. \tag{6}$$

Smith also showed that it was possible to calculate the branching ratios β_i, the probability of decay into a different asymptotic channel, using the square of the eigenvector associated with q_1, this information is also produced by TIMEDEL.

Fitting time-delays has a number of advantages over eigenphase sum fitting: fitting single eigenvalues removes most of the background which can be significant in molecular problems with many channels and, as discussed below, multiple time-delays can be studied for cases with overlapping resonances, a highly desirable property for ionic targets.

In the time-delay method, multiple resonances appear as interspersed Lorentzians in the highest eigenvalue, see figures 2 and 3. Discontinuities occur when the length of the time-delay of one resonance overtakes that of another; the eigenvalues associated with each resonance switch. Consequently, if only the first eigenvalue is fitted, information is lost when a resonance becomes the second and third eigenvalue. By including lower eigenvalues in the fitting procedure, a resonance can be tracked as it switches to lower eigenvalues, see figure 3. The second and third largest eigenvalues then provide the information that previously existed when only fitting the largest eigenvalue. Although this extra information is often unnecessary as Lorentzians are symmetric functions, it becomes important when the

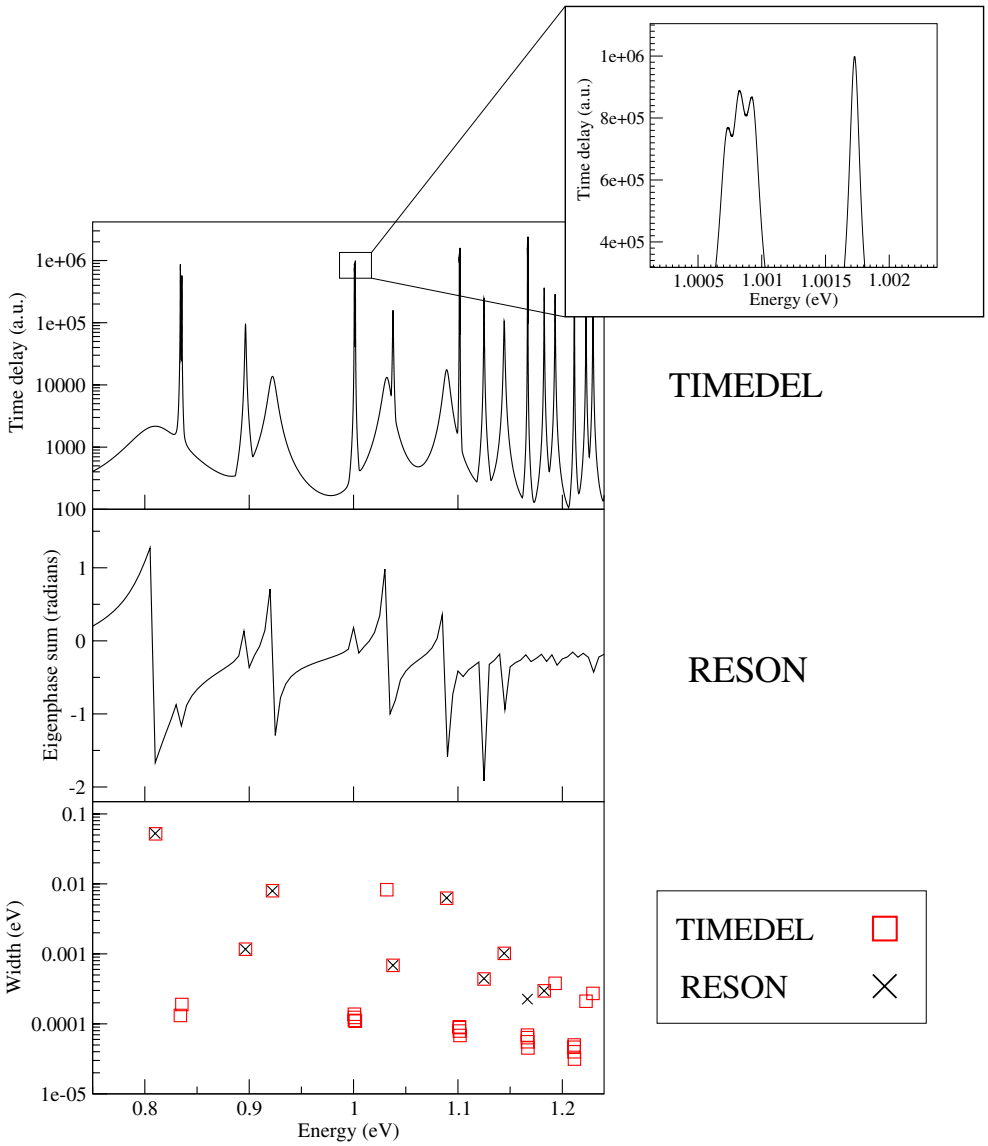

Figure 2. Comparison of the time-delay and eigenphase sum for the same energy range (top two panels) with fitted widths (lowest panel). The inset plot shows a zoom of one of the time-delay peaks. At high energies, close to the threshold, the resonances are narrow, close in energy, and overlap. As a result the eigenphase sum becomes impossible to interpret and unsuitable for fitting. The very fine energy grid used by TIMEDEL means that close-spaced narrow resonances, such as those shown in the inset plot, can be resolved. As shown in the plot of widths, the very narrow resonances ($\lesssim$0.2 meV), even at energies far from ($\sim$0.85 eV) the threshold are only detected by TIMEDEL.

peak of the resonance is in one of the lower eigenvalues. Indeed, this development reveals resonances that would have been previously left completely unidentified, those which have a similar position and marginally larger width to that of another resonance. The peak of a resonance of this type is within the second eigenvalue and only the tails switch into the first eigenvalue, see the magenta resonance in figure 3. Finding these resonances becomes particularly important when working in a lower symmetry group to that of the molecule under study; resonances that appear in the same (lower) symmetry group but actually have different symmetries may be obscured by one another. A new version of TIMEDEL was developed which includes fitting to the second and third eigenvalues where appropriate. Fits to further eigenvalues can easily be implemented but are not expected to be necessary. An updated version of the program will be published elsewhere (Little *et al* 2014).

This extension to the fitting method is the same concept as that introduced by Shimamura *et al* (2006). However, our method differs in that it is purely numerical and we did not formally derive an expression to describe overlapping resonances. Our fitting routine simply searches for minima in the difference between the eigenvalues and switches when one is found. Although this method is subject to occasional false detections, we have found it to be robust and to produce excellent fits.

The drawback of the time-delay method as implemented here is that there is no option but to scan an energy range to find the resonance positions and then only calculate the necessary points; the time-delay is simply calculated for a continuous range of energies to correctly locate and characterize the

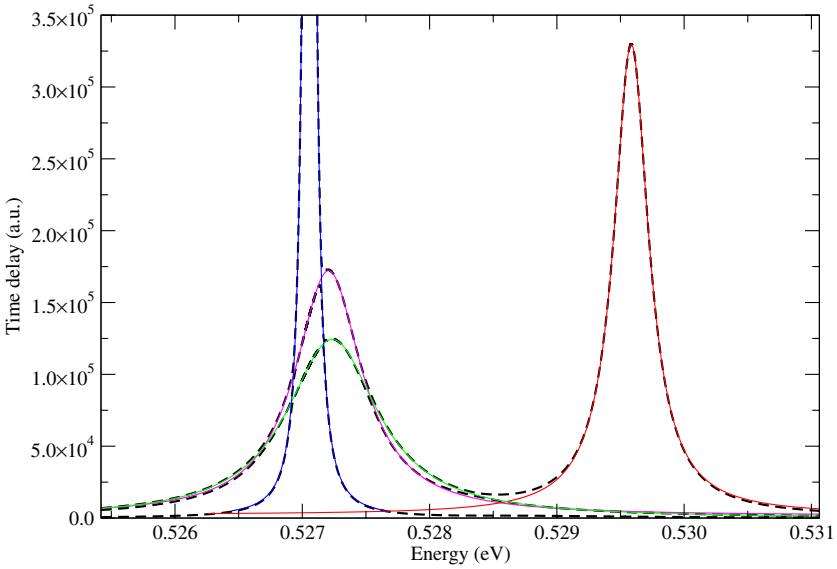

Figure 3. An example of fitting overlapping resonances using TIMEDEL. The dashed black lines are the largest three eigenvalues of the time-delay matrix, the continuous coloured lines are the fitted resonances. In the original implementation of TIMEDEL (Stibbe and Tennyson 1998) only the resonances coloured blue and red would have been fitted with reasonable accuracy. The magenta and green resonances would have been poorly fitted or missed entirely. By including the second and third eigenvalues in the fitting procedure, all of the resonances are well-fitted. Indeed, the green resonance would have remained undetected if the second and third eigenvalues had not been included in the fit.

resonances. As a result, when compared to fitting eigenphase sums, it is significantly more computationally expensive. However, if one is only interested in a particular dissociative curve the eigenphase sum can be quickly scanned at a number of internuclear separations to determine positions which can then be fitted to 'guide' a time-delay calculation. This combines the speed of eigenphase fitting and accuracy of the time-delay method. As **Q** is a numerical derivative, its computation requires two **K** matrices per energy, separated by a small energy gap, at most 10^{-5} eV, doubling the number of K-matrix calculations required in comparison to RESON. This becomes an issue close to thresholds where the resonant width becomes lower than the energy gap. Despite this, for the purposes of this study, the time-delay method has proven to give the most comprehensive and accurate results of the three methods discussed, see figure 1, and hence is our method of choice.

4.3. The QB method

The QB method (Quigley and Berrington 1996, Quigley *et al* 1998) is an R-matrix specific resonance-characterization procedure that takes advantage of the analytical properties of the R-matrix around a resonance. It was developed to be used for scattering from charged atomic targets and is based on the neglect of the outer region potential. Such potentials are significantly stronger in molecular ions so the QB method is not necessarily as accurate for molecules. It has, however, been suggested that in favourable circumstances the QB method should produce results similar to that of RESON and TIMEDEL (Ballance *et al* 1999). Homonuclear molecules such as nitrogen do not possess a permanent dipole moment so should be a favourable case. The QB method is analytic, so the inherent issues of a numerical calculation, robustness and numerical stability are avoided. The method is also computationally rapid and, unlike RESON and TIMEDEL which occasionally fail, in favourable circumstances provides complete sets of resonance.

In the QB method, the eponymous **Q** and **B** matrices are defined in terms of the asymptotic solutions, the R-matrix and energy derivatives so that, $\mathrm{d}\mathbf{K}/\mathrm{d}E = \mathbf{B}^{-1}\mathbf{Q}$. Eigenphase energy gradients of the **K** matrix can then be obtained; resonance positions are defined as the maximum gradient, the associated widths being related to the inverse of the eigenphase gradients.

Generally, the radius of the R-matrix sphere, a, is chosen to be large enough to enclose the target molecular charge cloud. For the QB method another issue has to be considered. Since the method neglects long-range potentials in the outer region, enlarging the inner region extends the range that these potentials are allowed for. In the case of N_2^+ the QB method gave, in most cases, positions and widths that were systematically lower than that given by both RESON and TIMEDEL, see figure 1. Attempts were made to improve the results by extending the R-matrix sphere to 15 a_0; although the resonance positions did change, they were still not comparable to those found by RESON and TIMEDEL. QB also did not detect a number of resonances associated with Rydberg states, see figure 1, the reason for this is unclear. As it was apparent that QB was not going to be suitable for this study no further investigation of this issue was undertaken.

5. Results and discussion

Resonances were calculated up to 6 eV above the equilibrium energy of the X state which restricts the range of internuclear separations to $R \approx 0.894$–1.818 Å; a grid of 0.001 Å was used. In principle the maximum calculable value of n

Table 3. Equilibrium energies, E_e (eV), internuclear separations, R_e (Å), and, quantum defects, α, of some Rydberg states converging upon excited states of N_2^+ compared to experiment. The equilibrium energy is given relative to the zero point energy of the X $^2\Sigma_g^+$ state. All states converge upon A $^2\Pi_u$ unless specified otherwise.

	This work			Experiment[a]		Comparison[b]	
State	E_e	R_e	α	E_e	α	ΔE_e	$\Delta\alpha$
$^3\Pi_u(5s\sigma_g)$	0.2914	1.182	1.1620	0.20	1.15	−0.0914	−0.0120
$^1\Pi_u(5s\sigma_g)$	0.3164	1.182	1.1093	0.25	1.05	−0.0664	−0.0593
$^3\Pi_u(6s\sigma_g)$	0.6327	1.182	1.1671	0.54	1.16	−0.0927	−0.0071
$^1\Pi_u(6s\sigma_g)$	0.6454	1.182	1.1136	0.57	1.03	−0.0754	−0.0836
$^1\Sigma_u^+(4s\sigma_g)$[c,d]	1.6017	1.085	1.0506	1.57	1.08	−0.0032	0.0294
$^1\Sigma_u^+(4d\sigma_g)$[c,d]	1.7942	1.087	0.8517	1.73	–	−0.0642	–

[a] Lofthus and Krupenie (1977).
[b] Obs. − Calc.
[c] Converges upon B $^2\Sigma_u^+$.
[d] Estimated as equilibrium position is close to A $^2\Pi_u$.

is only limited by numerical issues involving the energy difference used to calculate the numerical derivative of the time-delay matrix. In this study we chose to calculate up to $n = 10$. The raw data of position, width and quantum defect is available in the supplementary data (available at stacks.iop.org/JPhysB/47/105204/mmedia) in D_{2h} symmetry, all quantum defects are calculated relative to the closest threshold energetically. Rydberg states converging upon the a $^4\Sigma_u^+$ state should not be regarded as reliable since this ionic state was not optimized in our model and lies too high in energy. The state is included in the supplementary data (available at stacks.iop.org/JPhysB/47/105204/mmedia) to aid the identification of resonances that are not valid.

The choice of the lowest 100 target states in our close-coupling expansion is, of course, arbitrary and the actual states selected change as a function R due state crossings. As a result of this, beyond 1.466 Å there are significant numerical problems, that is, channels relating to Rydberg states dropping out of the calculation and discontinuities in PECs. PECs that remain smooth beyond 1.466 Å can be used as they are not affected by this state switch. Data relating to curves beyond 1.466 Å which appears noisy is probably best ignored. These target state crossings also cause some minor (∼0.02 eV) discontinuities in the resonance energy curves at shorter R.

Although in most cases TIMEDEL provides accurate robust fits, it is subject to false detections and poor fits due to the complications imposed by fitting overlapping resonances. In general it is obvious when there is a false detection or bad fit. A width which is very large or small in comparison to the other points making up the PEC can be discounted as a bad fit. However, significant changes in the magnitude of the width can occur as a state crosses a threshold and these should not be discounted.

5.1. Potential energy curves, quantum defects and shape resonances

Table 3 gives a comparison of equilibrium energies and quantum defects of the Rydberg states with the limited experimental data available. Agreement is generally good. We expect that the agreement with experiment will increase for higher n as can be seen for the recomputed $c_n'^1\Sigma_u^+$ series in table 1. The equilibrium energy of A $^2\Pi_u$ state is 0.078 25 eV above the experimental value given in Huber and Herzberg (1979) in our target model, this contributes to the disagreement with experiment of the Rydberg states converging on the A state. The equilibrium positions for the Rydberg states $^1\Sigma_u^+(4s\sigma_g)$ and $^1\Sigma_u^+(4d\sigma_g)$ were very close in energy and internuclear separation to the A $^2\Pi_u$ state. As TIMEDEL does not function reliably close to thresholds for reasons described in section 4.2, the equilibrium positions of these Rydberg states are only estimated.

Resonant states of singlet and triplet symmetries appear in figures 6 and 4 respectively. A comparison between our curves and those of Guberman (2012) is also given. These figures only give our results for resonance states which lie above the ion ground state. These curves join smoothly with the bound states lying below the ion, which are given in Little and Tennyson (2013). Although our curves largely appear to be solid lines, the resonant positions, coloured black, are simply represented by single points. The coloured lines from this work are the points joined together, no formal diabatization has been performed; the many avoided crossings are simply interpolated using a straight lines. Many states not presented by Guberman are also given. Full numerical data is given as supplementary material (available at stacks.iop.org/JPhysB/47/105204/mmedia) in D_{2h} symmetry. In most cases this data can be separated into $D_{\infty h}$ by matching up degenerate resonant positions. As this is a numerical technique the positions are not exactly degenerate. However, by considering the avoided crossings with other adiabats of the same symmetry and the quantum defects, symmetry assignments can be made unambiguously in almost all cases.

For the singlet states, the general agreement between our results and Guberman's is reasonable, except for the $b'^1\Sigma_u^+$ state. Our calculations suggest that this state is bound and does not appear above the ionization threshold, the position and shape of this curve in the bound region is in good agreement with that of Spelsberg and Meyer (2001), see Little and Tennyson (2013), adding confidence to this assertion. The position of Guberman's curve is similar to that of the $3d\pi_g$ Rydberg state converging on the B state. It is possible that due to the adiabatic nature of the MRCI approach that

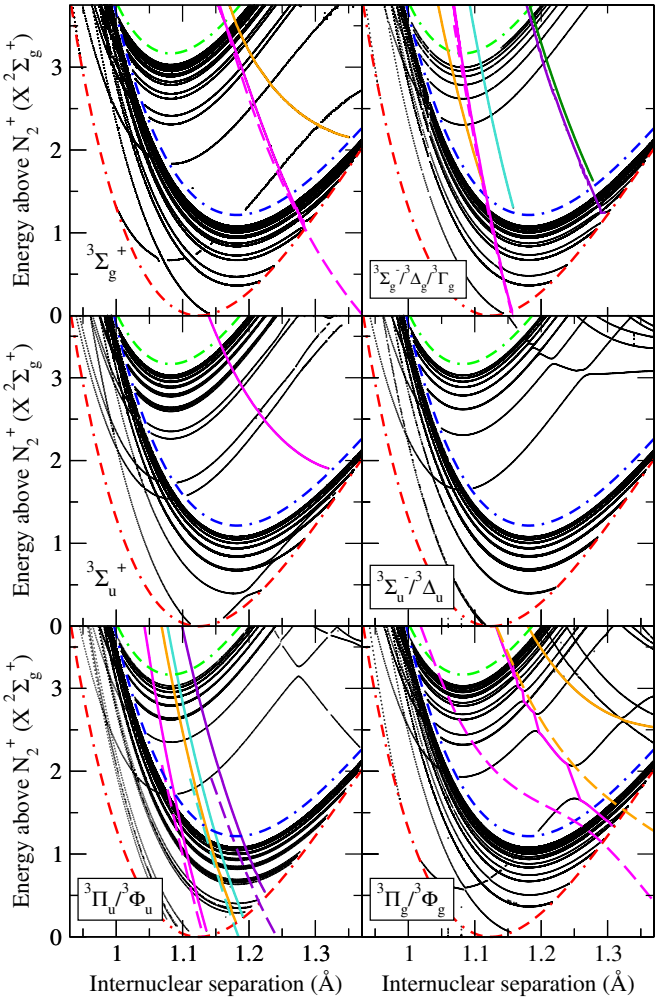

Figure 4. PECs for each of the triplet symmetries. Dashed and dotted lines are the N_2^+ states: $X\,^2\Sigma_g^+$ (red), $A\,^2\Pi_u$ (blue) and $B\,^2\Sigma_u^+$ (green). The dissociative valence states are highlighted in colour. In some cases Guberman has only presented a single curve of each symmetry and not assigned a letter or number prefix. In this case the curve corresponds to the curve in the this work with the prefix '1'. Solid lines are this work and broken lines are curves by Guberman (2012). Although the data series coloured in black showing the Rydberg states look like solid lines in places they are actually just single points in a dense grid of internuclear separations. The valence states are assigned as follows. $^3\Sigma_g^+$: — $1\,^3\Sigma_g^+$, — $2\,^3\Sigma_g^+$, — $3\,^1\Sigma_g^+$. $^3\Sigma_g^-/^3\Delta_g/^3\Gamma_g$: — $G\,^3\Delta_g$, — $1\,^3\Sigma_g^-$, — $2\,^3\Sigma_g^-$, — $3\,^3\Delta_g$, — $3\,^3\Sigma_g^-$. $^3\Sigma_u^+$: — $1\,^3\Sigma_u^+$. $^3\Pi_u/^3\Phi_u$: — $2\,^3\Pi_u$, — $H\,^3\Phi_u$, — $3\,^3\Pi_u$, — $4\,^3\Pi_u$. $^3\Pi_g/^3\Phi_g$: — $2\,^3\Pi_g$, — $3\,^3\Pi_g$.

the state presented in Guberman (2012) is a combination of this Rydberg state and the valence state. This highlights an advantage of using a scattering calculation to find the neutral states above the ionization threshold; it is easily seen that this state is part of a Rydberg series converging on the first excited state and not a valence state. This is confirmed by the narrow width of this state (∼5 meV) normally associated with Rydberg states.

Again for the triplet states the agreement with Guberman is generally good, with particularly good agreement for the $1\,^3\Sigma_g^+$ and $G\,^3\Delta_g$ states. The crossing point of the main DR dissociative channel, $2\,^3\Pi_u$, is similar. However, there is a large disparity between the shape and position of states of $3\,^3\Pi_g$ symmetry, such a large level of disagreement is unusual. As there is no experimental data for these states it is difficult to make a judgement as to which or even if either of these curves are correct.

Resonances of Σ^- symmetry are a special case. It is not possible to form Σ^- states by coupling a one-electron continuum orbital to the ground $X\,^2\Sigma_g^+$ state, so all states of $^1\Sigma_g^-$, $^1\Sigma_u^-$, $^3\Sigma_g^-$ and $^3\Sigma_u^-$ cannot autoionize below the threshold to the $A\,^2\Pi_u$ state. These resonances therefore become bound states in the continuum and are not detected by any of the resonance fitting techniques we employed. Since none of these resonances appear important for DR (for example they have zero coupling at low energies), we have not attempted to map out these states in the low-energy region and curves simply stop at the $A\,^2\Pi_u$ state, see examples of $^1\Sigma_g^-$ and $^3\Sigma_g^-$ in, respectively, figures 6 and 4 below. It should fairly straightforward to interpolate between our resonance curves and the bound states obtained previously if full curves are required.

'Intruder' states, also known as interloper resonances, are Rydberg states that appear below an ionic state below the one on which they converge; for N_2 they appear in all symmetries. The $^{1,3}\Sigma_g^+$ interloper resonances of N_2 have been described previously at a single internuclear separation by Ballance *et al* (1998). These interloper resonances are due to the close proximity in energy of the X, A and B states and lead to complicated state mixing as they overlap below each ionization threshold. As shown by Guberman (2007), interloper resonances play an important role in the dissociative recombination (DR) of N_2^+. The mixing of valence and Rydberg states above the B state suggests that it may be necessary to include the X, A and B cores and the Rydberg states that converge upon them to correctly describe the DR of N_2^+.

A recent study by Slaughter *et al* (2012) identified the signature of a shape resonance of $^3\Pi_u$ symmetry among the many Feshbach resonances in their electron – O_2^+ collision calculations. We therefore undertook a search for similar structures in molecular nitrogen. Initially our larger calculations suggested that this system may also support shape resonances. However these disappeared with the use of our more compact, linearly-independent basis sets suggesting that these features were an artefact of an over-complete basis. A number of test calculations failed to find conclusive evidence for these structures and we conclude that nitrogen, unlike oxygen, does not support any shape resonances.

Finally by matching the data using quantum defects, see Little and Tennyson (2013) for a more detailed description of this procedure, to form adiabats and combining it with bound adiabats from Little and Tennyson (2013) a complete picture of the electronic states of N_2 above and below the ionization threshold can be obtained, see figure 7. This figure shows that the R-matrix method can be used to create a comprehensive map of highly excited Rydberg-valence type neutral states for diatomic molecules and sets a benchmark for further calculations of this type.

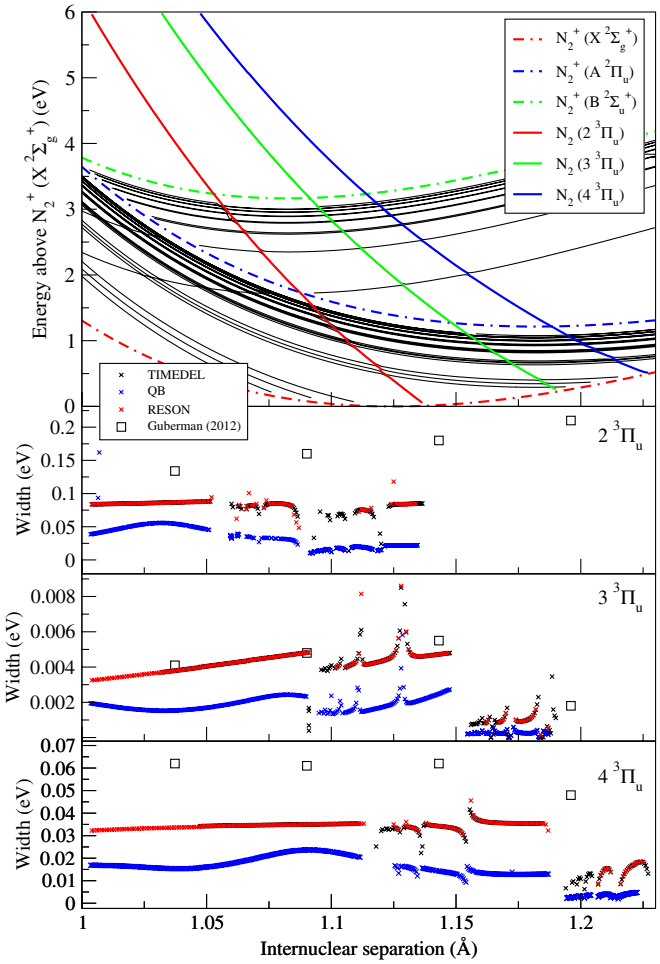

Figure 5. PECs of $^3\Pi_u$ symmetry with their respective widths and a comparison with widths calculated by Guberman (2012).

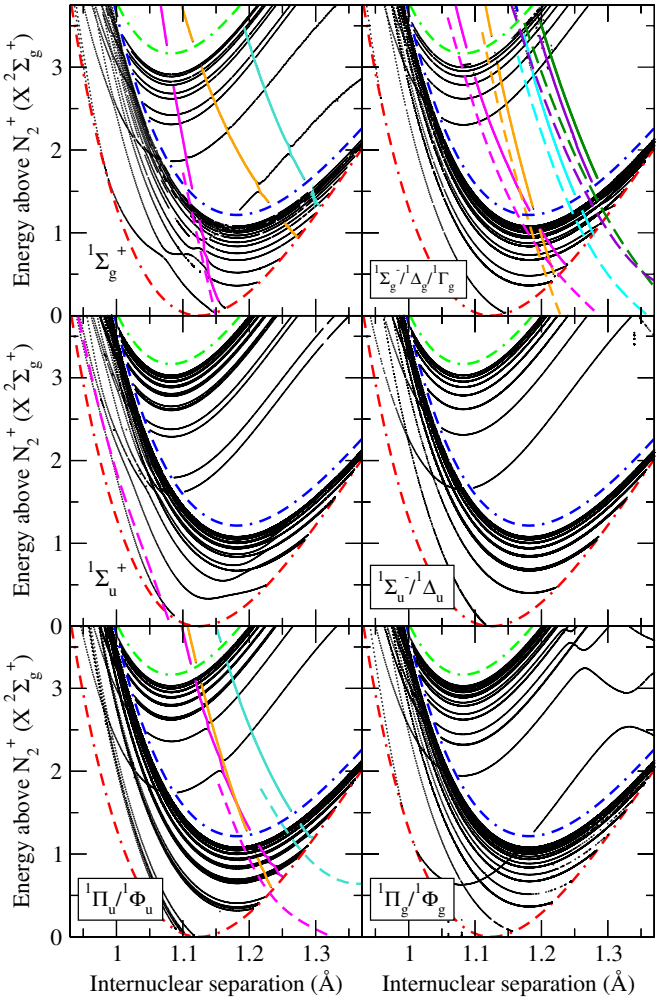

Figure 6. PECs for each of the singlet symmetries. Dashed and dotted lines are the N_2^+ states: $X\,^2\Sigma_g^+$ (red), $A\,^2\Pi_u$ (blue) and $B\,^2\Sigma_u^+$ (green). The dissociative valence states are highlighted in colour. Solid lines are this work and broken lines are curves by Guberman (2012). Although the data series coloured in black showing the Rydberg states look like solid lines in places they are actually just single points in a dense grid of internuclear separations. The valence states are assigned as follows. $^1\Sigma_g^+$: — $a''\,^1\Sigma_g^+$ (labelled as $2\,^1\Sigma_g^+$ by Guberman (2012)), — $2\,^1\Sigma_g^+$, — $3\,^1\Sigma_g^+$. $^1\Sigma_g^-/^1\Delta_g/^1\Gamma_g$: — $1\,^1\Delta_g$, — $1\,^1\Gamma_g$, — $2\,^1\Delta_g$, — $3\,^1\Delta_g$, — $1\,^1\Sigma_g^-$. $^1\Sigma_u^+$: — $b'\,^1\Sigma_u^+$ (in this work this state is bound and hence does not appear on the plot). $^1\Pi_u/^1\Phi_u$: — $2\,^1\Pi_u$, — $1\,^1\Phi_u$, — $3\,^1\Pi_u$.

5.2. Electronic resonance widths

Figure 5 gives a comparison of the three methods of resonance detection and a comparison with the widths of Guberman (2012) for the $^3\Pi_u$ symmetry. The $2\,^3\Pi_u$ state is the dominant dissociating channel in the DR of N_2^+ (Guberman 2012) and hence the magnitude of this width will have a significant effect on the cross-section. For reasons explained in section 4.3, the approximations made by the QB method are not suitable for N_2. This is reconfirmed by the widths being around half the magnitude of those found by RESON and TIMEDEL. RESON and TIMEDEL give the same positions and widths as they are calculated using the same K-matrices unlike the QB method. However, at the points where the states are interacting with others and overlapping significantly, for example above 1.19 Å in the plot of the $4\,^3\Pi_u$ state, RESON fails to resolve the position and width. TIMEDEL and RESON both reveal a significant amount of structure in the widths as they cross the Rydberg series converging on each threshold. The energy spacing of the Rydberg states is proportional to $^1/_{n^2}$, meaning that close to the threshold resolving individual resonances becomes intractable. The behaviour of the resonances is left undescribed slightly above and below each threshold. For resonant positions this is less of a problem as the shape of the PEC is generally predictable across the threshold. The behaviour of widths can change dramatically across a threshold as can be seen in figure 5; as the 3 and $4\,^3\Pi_u$ states cross the A state their width decreases significantly as the number of channels available for autoionization decreases.

To compare with widths calculated by Guberman (2012) we only include the open channels from the data provided above each threshold. That is, above the A state the widths are a sum of the X and A state widths and below the A state only the X state. For the 2 and $4\,^3\Pi_u$ states, Guberman's widths are systematically larger than ours and smooth. Conversely, agreement for the narrowest $3\,^3\Pi_u$ is good. We note that in Guberman's characterization, these resonances continue to have a width below the ionization threshold, in terms of the purely electronic behaviour considered here this is not possible

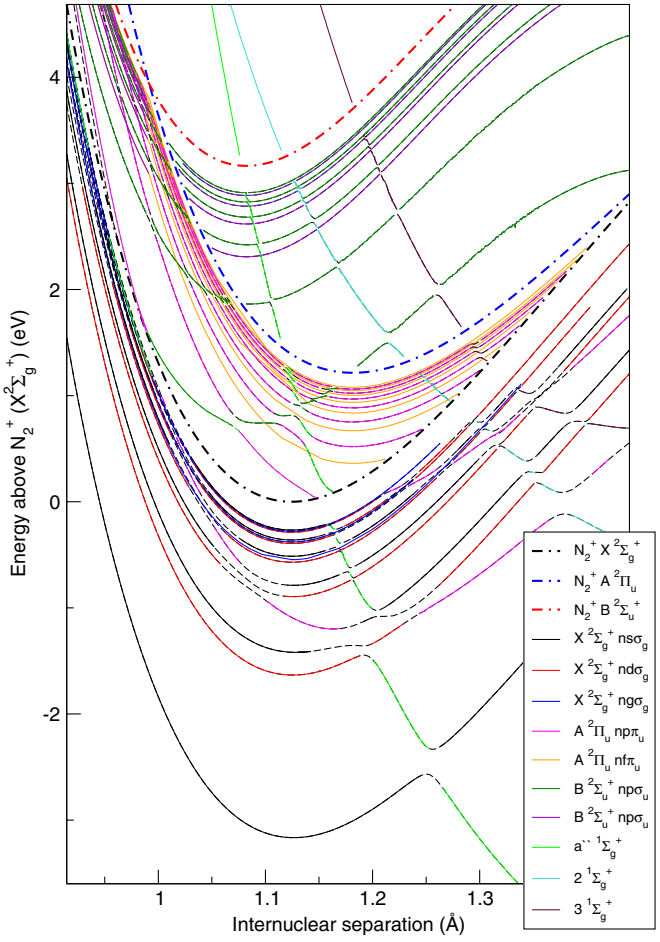

Figure 7. A complete description of the electronic structure of N_2 above and below the ionization threshold for states of $^1\Sigma_g^+$ symmetry. Data was matched by quantum defect to form adiabats, the colours show the diabatic states.

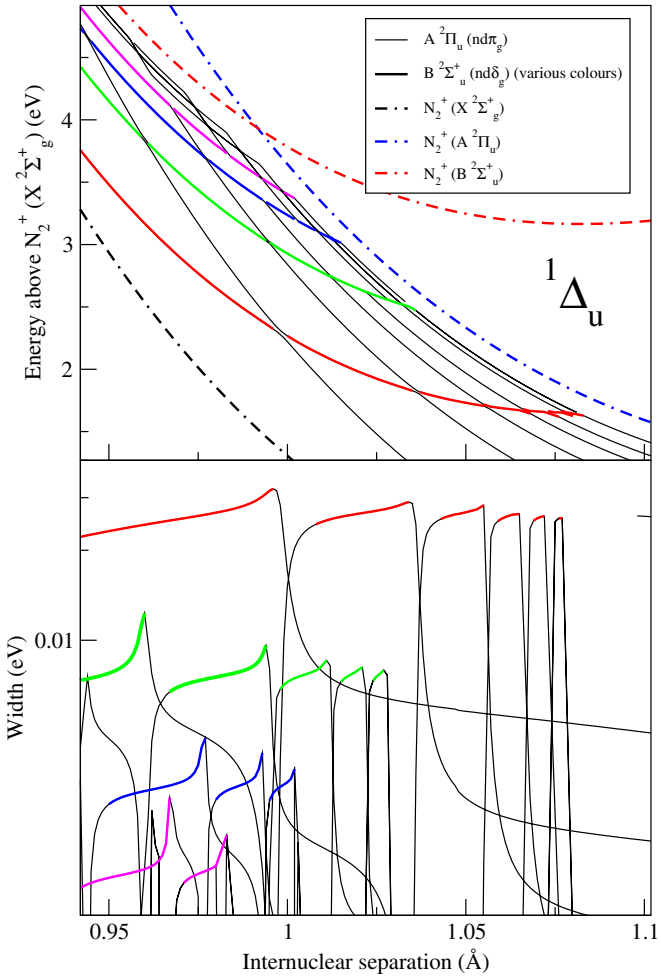

Figure 8. Interacting Rydberg series and their widths for total symmetry $^1\Delta_u$. On the top panel are the PECs of the $A\,^2\Pi_u$ ndπ$_g$ Rydberg series (narrow black lines) interacting with the $A\,^2\Pi_u$ ndδ$_g$ Rydberg series (thick coloured lines). Sections of the width-adiabats displayed in the lower panel are coloured coded to the Rydberg state they are associated with. The structure of the Rydberg series is represented in the widths as a series of plateaus decreasing in magnitude.

as bound electronic states have zero (electronic) widths. In general, we expect that the width of a resonance will decrease as the number of open channels decreases unless the width is dominated by a channel associated with the ground state. A decrease in open channels occurs as the state crosses a threshold. For the 3 and 4 $^3\Pi_u$ states there is a significant drop in width as they cross the B state, for 2 $^3\Pi_u$ the width remains fairly constant across the threshold showing that the dominant channel is associated with the X state. This decrease is seen in the 3 and 4 $^3\Pi_u$ states in Guberman's results whilst there is a general increase in resonance width with internuclear separation for the 2 $^3\Pi_u$.

Figure 8 shows PECs and widths for the $^1\Delta_u$(ndπ$_g$) and $^1\Delta_u$(ndδ$_g$) states converging on the A and B state respectively. This plot shows the detailed structure of the widths as these two Rydberg series interact. Each curve has been matched using quantum defect, the width-adiabat of each PEC has then been plotted in the lower panel. In this region of bond lengths, on average, the ndδ$_g$ series (coloured in the plot) has a larger width than that of the ndπ$_g$ series. As the ndδ$_g$ series crosses we see the width rapidly increase and plateau as it becomes the dominant electronic configuration of the adiabat and then rapidly decrease as it smoothly transitions back to ndπ$_g$. The Rydberg series itself is reflected in the structure of the widths, with a series of plateaus decreasing in size for each value of n. Even with the dense grid of internuclear separations used it is not fine enough for the plateaus close to the thresholds to be resolved. This kind of detailed width structure is only possible to obtain using TIMEDEL and a dense grid of internuclear separations.

5.3. Implications for a dissociative recombination cross-section calculation

The data presented here is extensive enough to provide detailed inputs to compute reliable DR cross-sections. The restriction of only calculating up to $n = 10$ should not have an effect on the cross-section. Although the widths of Rydberg states can be used in a DR cross-section calculation, the implementation we plan to use (Schneider *et al* 2000) only requires the input of quantum defects. We have shown in our previous study (Little and Tennyson 2013) that quantum

defects generally become stable for $n \geqslant 4$. As the R-matrix method works within the adiabatic Born–Oppenheimer approximation we cannot find the non-adiabatic coupling of the resonances, that is, energy dependent widths. For this molecule it is not expected that including the energy dependence of the widths would have any significant effect on the cross-section as the widths are generally narrow so energy-dependent effects are expected to be minimal. The most important dissociative state, $2\,^3\Pi_u$, has a similar crossing point to Guberman's and hence will dominate the cross-section. Therefore the most notable difference will be the impact of the narrower width of the $2\,^3\Pi_u$ state, use of this state in a DR calculation will inevitably lead to a reduction in the computed cross-section. The other two states which cross close to the X state equilibrium are the $a''\,^1\Sigma_g^+$ (labelled as $2\,^1\Sigma_g^+$ in Guberman (2012)) and $G\,^3\Delta_g$ states. These states have narrow widths at the crossing point ($\sim 10^{-3}$ eV and $\sim 10^{-4}$ eV respectively) and hence will only be minor dissociating channels. At higher electron energies, states which cross at higher energies will become important, however, there are no other states that have such a consistently large width as the $2\,^3\Pi_u$. Features from these minor dissociative routes will most likely appear as structures against the large background contribution from the $2\,^3\Pi_u$ state. This is where the main differences in the cross-section will be seen (aside from the overall magnitude due to the lower width of the $2\,^3\Pi_u$ state); there is disagreement between the crossing points of many of the minor dissociating channels which will have a significant effect on each of their individual cross-sections. Finally it would be interesting to see what effect the detailed structure of widths resolved by TIMEDEL will have on the DR cross-section.

6. Conclusion

We present three different methods for detecting and fitting singlet and triplet continuum states above the ionization threshold of N_2. The most comprehensive of these methods, the time-delay method, provided a highly detailed mapping of the resonance structure and widths. Comparison with the very limited experimental data available shows good agreement. The use of a dense grid and an improved fitting method reveals complicated structures in the widths and a description of their adiabatic nature with changing electronic configuration. Neutral states which could provide routes to dissociation in a DR calculation have been identified and compared with those given by Guberman (2012). In general agreement in position for the main dissociative states is good, but we have found narrower widths with much more pronounced structure. These differences should effect calculated DR cross-sections.

We plan to use the combined data from this study and Little and Tennyson (2013) to calculate the DR cross-section N_2^+. The good agreement we found with experimental data in this study and the previous indicates that it may not be necessary to empirically alter our data in order to successfully model DR as was the case in previous studies (Schneider *et al* 2000). It will be interesting to see what effect the detailed structure of the widths has upon the cross-section. Finally this study of DR will provide a direct comparison between two different methods of generating data for a DR calculation; an MRCI based approached and an R-matrix approach.

Acknowledgments

We thank Themisys Limited for supporting a studentship for DAL. We thank A Sunderland and M Plummer for provision of computer time. DAL would also like to acknowledge C Sousa-Silva and A F Al-Refaie for their support and helpful discussions.

References

Baccarelli I, Sebastianelli F, Gianturco F A and Sanna N 2009 *Eur. Phys. J.* D **51** 131–6
Ballance C P, Berrington K A and McLaughlin B M 1999 *Phys. Rev.* A **60** R4217
Ballance C P, McLaughlin B M, Nagy O, Berrington K A and Burke P G 1998 *J. Phys. B: At. Mol. Opt. Phys.* **31** L305
Canosa A, Gomet J C, Rowe B R and Queffelec J L 1991 *J. Chem. Phys.* **94** 7159–63
Carr J M, Galiatsatos P G, Gorfinkiel J D, Harvey A G, Lysaght M A, Madden D, Masin Z, Plummer M and Tennyson J 2012 *Eur. Phys. J.* D **66** 58
Cunningham A J and Hobson R M 1972 *J. Phys. B: At. Mol. Opt. Phys.* **5** 2328
Dora A, Bryjko L, van Mourik T and Tennyson J 2009 *J. Chem. Phys.* **130** 164307
Dunning T H 1989 *J. Chem. Phys.* **90** 1007–23
Faure A, Gorfinkiel J D, Morgan L A and Tennyson J 2002 *Comput. Phys. Commun.* **144** 224–41
Geoghegan M, Adams N G and Smith D 1991 *J. Phys. B: At. Mol. Opt. Phys.* **24** 2589
Guberman S 2003 *Dissocative Recombination of Molecular Ions with Electrons* (New York: Kluwer/Plenum) pp 187–196
Guberman S L 2007 *J. Phys. Chem.* A **111** 11254–60
Guberman S L 2012 *J. Chem. Phys.* **137** 074309
Guberman S L 2013 *J. Chem. Phys.* **139** 124318
Hazi A U 1979 *Phys. Rev.* A **19** 920–922
Huber K and Herzberg G 1979 *Constants of Diatomic Molecules* (New York: Van Nostrand Reinhold) http://webbook.nist.gov
Huber K P and Jungen C 1990 *J. Chem. Phys.* **92** 850–61
Larsson M and Orel A E 2008 *Dissociative Recombination of Molecular Ions (Cambridge Molecular Science)* (Cambridge: Cambridge University Press)
Little D A *et al* 2014 in preparation
Little D A and Tennyson J 2013 *J. Phys. B: At. Mol. Opt. Phys.* **46** 145102
Lofthus A and Krupenie P H 1977 *J. Phys. Chem. Ref. Data* **6** 113–307
Mahdavi M R, Hasted J B and Nakshbandi M M 1971 *J. Phys. B: At. Mol. Opt. Phys.* **4** 1726
Masin Z and Gorfinkiel J D 2012 *J. Chem. Phys.* **137** 204312
Mehr F J and Biondi M A 1969 *Phys. Rev.* **181** 264–71
Morgan L A, Gillan C J, Tennyson J and Chen X 1997 *J. Phys. B: At. Mol. Opt. Phys.* **30** 4087–96
Mul P M and McGowan J W 1979 *J. Phys. B: At. Mol. Phys.* **12** 1591
Nagy O 2003 *Chem. Phys.* **286** 109–14
Nagy O, Ballance C P, Berrington K A, Burke P G and McLaughlin B M 1999 *J. Phys. B: At. Mol. Opt. Phys.* **32** L469
Orel A E, Rescigno T N and Lengsfield B H 1990 *Phys. Rev.* A **42** 5292–7
Peterson J R *et al* 1998 *J. Chem. Phys.* **108** 1978–88

Quigley L and Berrington K 1996 *J. Phys. B: At. Mol. Opt. Phys.* **29** 4529–42
Quigley L, Berrington K and Pelan J 1998 *Comput. Phys. Commun.* **114** 225–35
Rabadán I, Tennyson J and Morgan L A 1998 *Chem. Phys. Lett.* **285** 105–13
Rescigno T, McCurdy C, Orel A and Lengsfield B H I 1995 *Computational Methods for Electron—Molecule Collisions* ed W Huo and F Gianturco (Berlin: Springer) pp 1–44
Schneider I F, Rabadán I, Carata L, Tennyson J, Andersen L H and Suzor-Weiner A 2000 *J. Phys. B: At. Mol. Opt. Phys.* **33** 4849–61
Sheehan C H and St-Maurice J P 2004 *J. Geophys. Res.: Space Phys.* **109** A03302
Shimamura I 2011 *J. Phys. B: At. Mol. Opt. Phys.* **44** 201002
Shimamura I 2012 *Advances in Quantum Chemistry* (*Advances in Quantum Chemistry* vol 63) ed C A Nicolaides, E Brndas and J R Sabin (New York: Academic) pp 165–245
Shimamura I, McCann J F and Igarashi A 2006 *J. Phys. B: At. Mol. Opt. Phys.* **39** 1847–54
Slaughter D S, Adaniya H, Rescigno T N, Haxton D J, McCurdy C W, Belkacem A, Larson and Orel A E 2012 *J. Phys. Conf. Ser.* **388** 012016
Smith F T 1960 *Phys. Rev.* **118** 349–56
Sochi T and Storey P J 2013 *Eur. Phys. J. Plus* **128** 82
Spelsberg D and Meyer W 2001 *J. Chem. Phys.* **115** 6438–49
Stibbe D T and Tennyson J 1996 *J. Phys. B: At. Mol. Opt. Phys.* **29** 4267–83
Stibbe D T and Tennyson J 1998 *Comput. Phys. Commun.* **114** 236–42
Stibbe D T and Tennyson J 1999 *Chem. Phys. Lett.* **308** 532–6
Tennyson J 1996a *J. Phys. B: At. Mol. Opt. Phys.* **29** 1817–28
Tennyson J 1996b *J. Phys. B: At. Mol. Opt. Phys.* **29** 6185–201
Tennyson J 2010 *Phys. Rep.* **491** 29–76
Tennyson J and Noble C J 1984 *Comput. Phys. Commun.* **33** 421–4
Werner H J *et al* 2010 MOLPRO, a package of *ab initio* programs see www.molpro.net/
Zipf E C 1980 *Geophys. Res. Lett.* **7** 645–8